Nanoscale Noncontact Subsurface Investigations of Mechanical and Optical Properties of Nanoporous Low-*k* Material Thin Film

Alexey M. Lomonosov,[†,⊥] Adil Ayouch,[†] Pascal Ruello,[†,*] Gwenaelle Vaudel,[†] Mikhail R. Baklanov,[‡] Patrick Verdonck,[‡] Larry Zhao,[§] and Vitalyi E. Gusev[†,*]

[†]Laboratoire de Physique de l'Etat Condensé, UMR 6087 CNRS—Université du Maine, Le Mans, France, [‡]IMEC, Kapeldreef 75, B-3001 Leuven, Belgium, and [§]GLOBALFOUNDRIES assignee at IMEC, Kapeldreef 75, B-3001 Leuven, Belgium. [⊥]On leave from the General Physics Institute, Russian Academy of Sciences, Moscow, Russia.

ABSTRACT

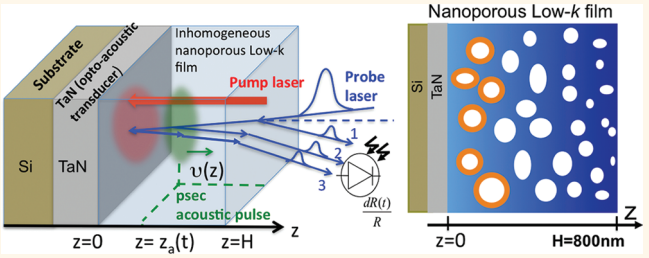

Revealing defects and inhomogeneities of physical and chemical properties beneath a surface or an interface with in-depth nanometric resolution plays a pivotal role for a high degree of reliability in nanomanufacturing processes and in materials science more generally.[1,2] Nanoscale noncontact depth profiling of mechanical and optical properties of transparent sub-micrometric low-*k* material film exhibiting inhomogeneities is here achieved by picosecond acoustics interferometry. On the basis of the optical detection through the time-resolved Brillouin scattering of the propagation of a picosecond acoustic pulse, depth profiles of acoustical velocity and optical refractive index are measured simultaneously with spatial resolution of tens of nanometers. Furthermore, measuring the magnitude of this Brillouin signal provides an original method for depth profiling of photoelastic moduli. This development of a new opto-acoustical nanometrology paves the way for in-depth inspection and for subsurface nanoscale imaging of inorganic- and organic-based materials.

KEYWORDS: picosecond laser ultrasonics · nanoacoustics · acousto-optics · depth profiling · transparent films · low-permittivity films

Spatial in-depth nonuniformity of thin solid films is becoming a critical factor with the aggressive down-scaling of their thickness. The most crucial reason for the nonuniformity is related to the different mechanisms of chemical reactions occurring in the bulk and at interfaces and to the increasing surface/volume ratio. Many different examples demonstrate this statement. For instance, the Young modulus of polycrystalline diamond films grown by microwave-[3] or e-beam-assisted[4] chemical vapor deposition continuously varies from the nucleation side to the growth side. The variation in the film texture with the increasing film thickness is considered a common phenomenon for film growth in general.[5] The variations of the material properties inside the film can take place at the scales from a few nanometers to hundreds of nanometers.[3−5] Inhomogeneity of thin films can also be caused by their postdeposition processing such as radiation-assisted curing used in the fabrication of low dielectric constant (low-*k*) films for modern microelectronic devices.[6−10] In addition, inhomogeneity can be introduced intentionally for the production of multilayered optical antireflective and highly reflective coatings.[11] For these UV optics the individual layers, constituting the coating, are of nanoscale thickness.

Several techniques allow inspection of the physical and chemical properties of solids with a nanometric resolution. Scanning probe microscopy (SPM[12]) is routinely employed, but it is limited to surface investigation. When subsurface information is required, invasive treatments are usually needed. Typically, sub-nanometer resolution images of the microstructure are obtained after sample microtoming (cross section image with transmission electron microscopies[13]). In-depth chemical and physical analysis can also be performed by slicing the material and analyzing either the removed matter (secondary ion mass spectroscopy[14]) or the newly created surface (ion-sputtering-assisted X-ray and ultraviolet photoemission

* Address correspondence to vitali.goussev@univ-lemans.fr, pascal.ruello@univ-lemans.fr.

Received for review November 1, 2011 and accepted January 1, 2012.

Published online January 02, 2012
10.1021/nn204210u

spectroscopy[15]). Because of the importance of nanometrology development for industry, special efforts are still needed to realize a breakthrough in subsurface investigation methods. As an illustration, recent developments of new modes in atomic force microscopy using the nonlinear mechanical interaction between an oscillating tip and the sample surface[16,17] have allowed for the first time a 50 nm subsurface investigation of mechanical properties.[18,19] So far, there are no noncontact nondestructive methods available to evaluate depth profiles of the mechanical and optical properties of sub-micrometer thick films with nanoscale spatial resolution.

RESULTS AND DISCUSSION

Recently, it has been proposed[20] that the in-depth distribution of the elastic modulus in transparent films could be determined using picosecond ultrasonic interferometry.[21] This opto-acoustic ultrafast pump–probe technique includes thermoelastic excitation of a picosecond acoustic pulse by a pump femtosecond laser pulse and monitoring the propagation of this acoustic pulse inside a transparent film by measuring the optical intensity reflectivity changes, $\Delta R(t)/R$, of the time-delayed probe femtosecond laser pulses (Figure 1) ($\Delta R(t)$ is the transient change of the optical intensity reflection coefficient, and R is the reflectivity of the undisturbed sample). In the particular situation depicted in Figure 1a, which is the configuration of our current investigations, the strain pulse emitted into the transparent film due to thermal expansion of the laser-heated TaN film, has a spatial length of about 10 nm. Due to acousto-optic interactions, the strain pulse scatters a part of the probe laser radiation penetrating into the transparent film (an example of the radiation scattered by the acoustic pulse is beam 2 in Figure 1a). As the strain pulse is propagating, the phase shift between the probe radiation scattered by the strain pulse and the probe radiation scattered by the surface (see beam 1 in Figure 1a) and the interfaces (for example beam 3 in Figure 1a) of the tested structure continuously changes in time. Because of this, the interference of all reflected optical probe rays at the photodetector induces a sinusoidally oscillating contribution to the optical intensity reflectivity changes $\Delta R(t)/R$ presented in Figure 1b (these Brillouin oscillations are solely presented in the inset of Figure 1 b). In the situation depictured in Figure 1a the acoustic pulse is reflected at the mechanically free surface of the transparent layer at time $t = \Delta t_{echo}$ (see Figure 1b). As demonstrated in the present paper, the typical frequency of this Brillouin oscillation, the so-called Brillouin frequency $f_B(t)$, is not constant in spatially inhomogeneous medium (see Figure 1c and Figure 2a). At a particular instant t of time, due to the relation $f_B(t) = 2v(t)[n^2(t) - \sin^2(\theta)]^{1/2}/\lambda$ (where λ and θ denote the optical wavelength in a vacuum and the incidence

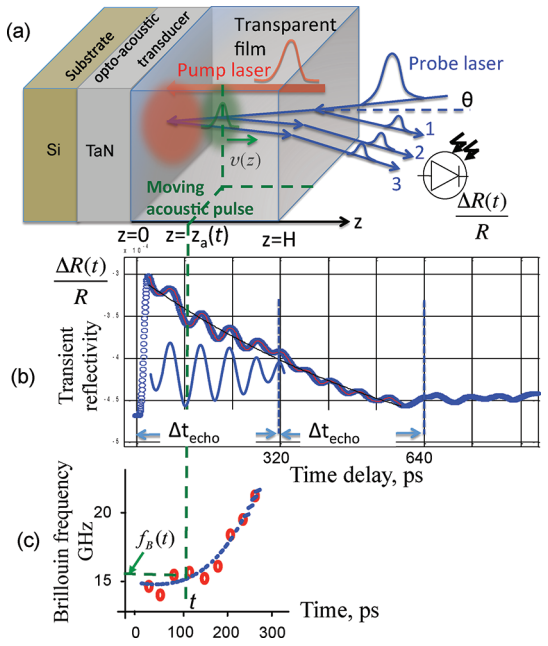

Figure 1. Qualitative illustration of the physical principles of the transparent media depth profiling. (a) Pump laser (in red) excites acoustic pulse (in green) of about 10 nm spatial length. This acoustic pulse scatters probe laser pulses, which are measuring the transient optical reflectivity of the sample. (b) The transient reflectivity signal d$R(t)/R$ contains an oscillatory contribution, the so-called Brillouin oscillations. (c) Both the amplitude and the frequency of the Brillouin oscillations in spatially inhomogeneous media are not constant. (d) The Brillouin frequency at a particular time point contains information on the material properties in the spatial point where the acoustic pulse is located at this time point.

angle of the probe radiation, respectively), it contains information both on the velocity of the acoustic pulse $v(z = z_a(t))$ and on the optical reflective index $n(z = z_a(t))$ at the coordinate $z = z_a(t)$ where the acoustic pulse is located (see Figure 1a). Here we demonstrate that by performing picosecond ultrasonic interferometry at a few angles θ of probe light incidence[22,23] it is straightforward to determine from the detected $f_B(t)$ the profile of the refractive index $n(z)$ simultaneously with the profile of the sound velocity $v(z)$. Moreover, by monitoring the variation in time of the amplitude $A_B(t)$ of the Brillouin oscillation, the spatially inhomogeneous profile of the photoelastic coefficient $P(z)$ is characterized. To present an example of the functionalities and facilities of the technique, we have conducted experiments in low-k nanoporous films, the new insulating dielectric materials for microelectronics interconnects. This transparent film exhibits in-depth inhomogeneities as a result of the manufacturing process. These inhomogeneities come from a nonuniform in-depth thermally assisted UV curing process that is fully described in the Supporting Information. Because of nonuniform UV absorption within the transparent film that inhibits perfect UV curing simultaneously at all depths, nonuniform in-depth dependence of the chemical

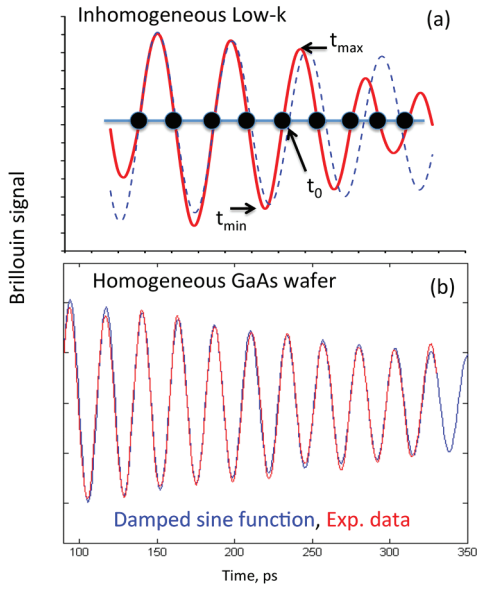

Figure 2. (a) Brillouin oscillations (red curve), extracted from the reflectivity signal of inhomogeneous nanoporous film, show a clear departure from a pure sine function (dashed blue curve), demonstrating the existence of spatial inhomogeneities within the thin film. (b) Brillouin oscillations (red curve), extracted from the reflectivity signal of homogeneous GaAs single crystals, are perfectly fitted with a sinus function (blue curve), demonstrating subsurface homogeneity.

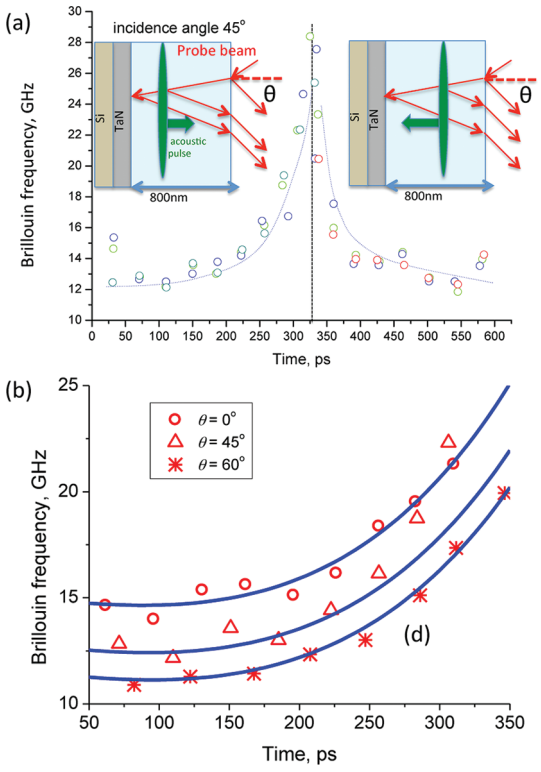

Figure 3. (a) Time dependence symmetry of the Brillouin frequency extracted from the transient reflectivity signal for forward and backward traveling acoustic pulse. The different colored symbols correspond to different experiments (the blue dashed lines are guide for eyes). (b) Extraction of time-dependent Brillouin frequency of the transient reflectivity signal obtained at different probe beam incidence angle θ. The data processing for extraction is explained in Methods.

composition (porogen content) and the UV-induced matrix cross-linkage, causing an increase in both rigidity and density of the material, appear as qualitatively depicted in Figure 4a.[10]

In the pump−probe experiment, the 200 fs long pump laser pulses with a repetition rate of 76 MHz from a Ti:sapphire laser are partially absorbed in the TaN layer, playing a role of opto-acoustical transducer, to generate picosecond strain pulses, which propagate through the low-*k* layer and interact with light of the probe laser beam. For the pump the wavelength of 880 nm was used, and its second harmonic (440 nm) was used as the probe. The spatial resolution, controlled by half of the Brillouin period ($\Lambda_B = v/f_B$), is $\Lambda_B/2 \approx 80$ nm, which is sufficient to reveal the important inhomogeneity of the 800 nm thick film. The detailed Brillouin signal obtained for the inhomogeneous nanoporous film, shown in Figure 2a, exhibits a clear departure from a simple sine function (dashed line). As a relevant comparison, a transient reflectivity signal obtained for an in-depth homogeneous semi-infinite EPI-ready GaAs wafer is shown in Figure 2b, where the experimental Brillouin oscillation obtained with a pump and probe wavelength of 800 nm (in red) is perfectly described by a damped sinus function (in blue). The Brillouin signal has a constant frequency of 42.5 ± 0.2 GHz over the measured depth of around 1 μm within a spatial resolution of $\Lambda_B/2 \approx 50$ nm. Moreover, as a proof of the reliability of the experimental observations, the Brillouin frequency determined in inhomogeneous low-*k* film for a forward ($0 < t < \Delta t_{echo}$) and backward ($\Delta t_{echo} < t < 2\Delta t_{echo}$) traveling acoustic pulse is perfectly symmetric in time (see Figure 3a).

For the quantitative extraction of in-depth physical properties from the time-resolved Brillouin light-scattering process determined through the transient reflectivity $\Delta R(t)/R$, we assume that the material parameters of the low-*k* film are varying only with the depth coordinate *z*. Under the assumption of small variations of the mechanical parameters within the spatial width of the strain pulse, the method of the slowly varying pulse profile[24] provides a quantitative description of evolution of a strain pulse in a medium. As the strain pulse with initial amplitude $\eta(0)$ and duration τ propagates along the *z*-axis from the transducer at $z = 0$ toward the outer surface at $z = H$ (Figure 1a) in a medium with nonuniform density $\rho = \rho(z)$ and longitudinal acoustic velocity $v = v(z)$, its magnitude varies as

$$\eta(z) = \eta(0)\left(\frac{v(z)}{v(0)}\right)^{-3/2}\left(\frac{\rho(z)}{\rho(0)}\right)^{-1/2} \quad (1)$$

and its spatial width varies as $\tau v(z)$. Under the assumption that the propagation of the probe light

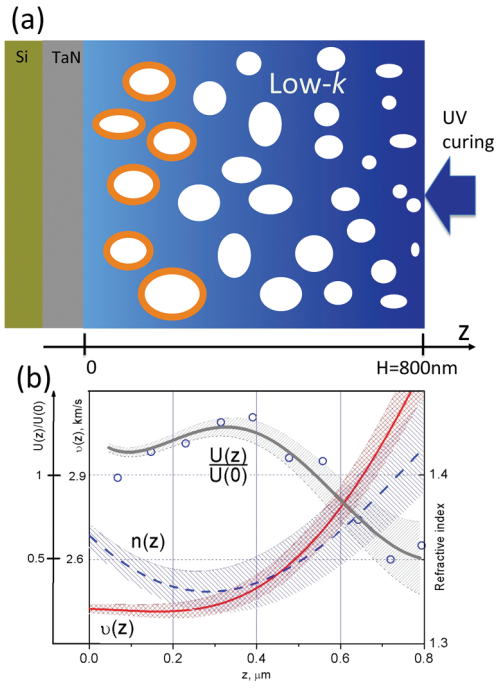

Figure 4. (a) Representation of the sub-micrometric inhomogeneities that exist within our prototype transparent film. These inhomogeneities are the result of the thermally assisted UV curing that is described in detail in the Supporting Information. The white disks are nanopores. Their dimension varies from the free surface toward the TaN–low-k interface. The blue matrix is organo-siloxane medium. The color gradient indicates that the deeper (lighter) blue is the region of higher (smaller) elastic modulus. Some nanopores still contain polymeric porogen (orange edge of pores) that was not completely removed during nanomanufacturing. (b) Depth profiles of the refractive index, $n(z)$, the sound velocity, $\upsilon(z)$, and the normalized photoelastic coefficient, $P(z)/P(0) \approx U(z)/U(0)$, obtained by opto-acoustic nanometrology. The data processing for the estimation of the standard deviations of these parameters, marked by shaded areas in (b), is explained in Methods.

waves in an inhomogeneous film can be described within the frame of geometrical optics[25] and that the short acoustic pulse can be described by a delta-localized acoustic pulse, $\eta(z,t) = \eta(z)\tau\upsilon(z)\delta[z-z_\alpha(t)]$,[26] the solution for the relative variations of the reflected probe intensity takes the following general form:

$$\frac{\Delta R(t)}{R} \cong 2\mathrm{Re}\left\{ B(t) + iK\frac{\eta(0)\tau}{k\sqrt{n^2(z_a) - \sin^2(\theta)}}\frac{P(z_a)}{\sqrt{\upsilon(z_a)\rho(z_a)}}\left[e^{2iS(z_a)} + r^2 e^{-2iS(z_a)}\right]\right\} \quad (2)$$

Here k stands for the probe wavenumber in a vacuum, r is the reflection coefficient of the optical field incident from the transparent film on the metallic film, K is a complex-valued constant, and $B(t)$ is a complex-valued function, which accounts for the slow displacements of the low-k film surfaces and the evolution of TaN layer temperature. $P(z)$ is the depth-dependent photoelastic coefficient. The optical eikonal S is determined by the refractive index distribution along the optical path: $S(z) = k\int_0^z [n^2(z') - \sin^2\theta]^{1/2}dz'$. The Brillouin frequency is derived from S according to $f_B(t) = (\partial/\partial t)[2S(z_a)] = (1/\pi)\upsilon(z_a)k[n^2(z_a) - \sin^2(\theta)]^{1/2}$. Moreover, because of the variations of the strain pulse amplitude (eq 1) and its spatial extension $\upsilon(z)\tau$ along z, the Brillouin oscillations magnitude $A_B(t)$ is time-dependent:

$$A_B(t) \propto \frac{1}{\sqrt{n^2(z_a) - \sin^2(\theta)}}P(z_a)\frac{1}{\sqrt{\upsilon(z_a)\rho(z_a)}} \quad (3)$$

Formally, it follows that, once the Brillouin frequency $f_B(t)$ is extracted from $\Delta R(t)/R$ (see Methods), the depth dependencies of $\upsilon(z)$ and $n(z)$ can be evaluated by measuring $f_B(t)$ at only two different angles θ and solving the obtained system of equations. In practice, however, this method is not applicable, because the frequency is sampled at discrete time instances $t_i(\theta)$, which are different for the different angles θ. In this case it is preferable to solve the overdetermined system of equations, because the larger number of equations provides higher accuracy (see Methods). In our case the time-dependent Brillouin frequency was measured for three different angles ($\theta = 0°$, 45°, and 60°; see Figure 3b). Extracted $\upsilon(t)$ and $n(t)$ have been transformed, using the space–time correspondence $z = z_a(t) = \int_0^t \upsilon(t')\,dt'$, into the in-depth distributions $\upsilon(z)$ and $n(z)$ (Figure 4b). With the evaluated variations of the acoustic velocity and the refractive index at hand, the amplitudes of the Brillouin oscillation $A_B(t_j)$ were used to examine variations in space of the parameter $U(z) = P(z)/[\rho(z)]^{1/2}$. In particular, for normal incidence of the probe, $U(z) \propto A_B(z)\, n(z)/[\upsilon(z)]^{1/2}$ (normalized form $U(z)/U(0)$ in Figure 4b).

The experimental results presented in Figure 4b reveal a wealth of nanoscale subsurface information. The gradient of $\upsilon(z)$ reaches 30%, whereas $n(z)$ exhibits significantly smaller variations of about 6% consistently with reports of a significant influence of the curing stage on the stiffness[8] (up to a 4-fold increase), on the refractive index[10] (7% reduction), and on the mass density[10] (23% increase). Experimentally revealed nonmonotonic variations of the optical density n along the depth coordinate z of the nanoporous low-k film are correlated by us with its nonmonotonic dependence on the dose of the UV radiation, which assists film curing (see Supporting Information). Parameter $U(z)$ also exhibits a nonmonotonic distribution over depth, but in an inverse way compared to $n(z)$, reaching minima at both sides of the film. $U(z)$ increases up to 30% of its low-k–TaN interface value halfway through the film but subsequently decreases down to 60% of that value at the surface. Density is expected to increase toward the outer surface by no more than 23%.[10] This could induce a maximum 11.5% change of $U(z)$ at the surface. Thus, the photoelastic coefficient $P(z)$ is the dominant contributor to the variations of

$U(z)$, and its depth dependence has qualitatively the same shape as is shown in Figure 4b for $U(z)$. The photoelastic coefficient is found to be the most sensitive to low-k film spatial inhomogeneity among the other evaluated material parameters.

CONCLUSIONS

To conclude, our proposed method demonstrates that it is possible to reveal reliable nanoscale in-depth profiles of elastic properties without using invasive methods as previously employed for low-k films.[8] Moreover, we supply additional information both on the refractive index and on the photoelastic coefficient consistently with the physical and chemical in-depth modifications that the UV-assisted thermal curing introduces (see Supporting Information). We have presented above the results where the spatial resolution (of about 80 nm) is limited by the half-wavelength of hypersound at the Brillouin frequency, because of a particular applied robust data processing method involving averaging over half of the Brillouin period. However, in perspective, the spatial resolution can be improved by an order of magnitude (down to 10 nm length scale of the picosecond acoustic strain pulse generated in a TaN opto-acoustic transducer of 30 nm thickness) by improving signal processing. Moreover, the application of depth profiling of the acoustic waves generated in sub-nanometer-thick opto-acoustic transducers is expected to provide sub-nanometer depth resolution. This new nanometrology approach could have important applications in opto-acoustic imaging and in nondestructive noncontact evaluation of transparent nanomaterials and nanostructures as well as of biological systems.

METHODS

Extraction of Local Brillouin Frequency. The complexity of the physical processes generalized in $B(t)$ (eq 1) makes it difficult to model it analytically. In this work we make use of the assumption of the relative slowness of $B(t)$, so that within half an oscillation period it can be approximated as $B(t) \approx bt + c$. This allows the effective elimination of the slow term. The procedure consists of two iteration steps. First, local minima and maxima of the signal are found. Each adjacent pair of them, say $t_{\min}^{(j)}$ and $t_{\max}^{(j)}$, limits the jth half-period of the Brillouin oscillation (see Figure 2a). Within this interval the signal is represented as a sum of a sinusoidal signal and a piecewise approximated $B(t)$: $s(t) = A_B\sin(2\pi f_B t + \phi) + bt + c$, with five unknown parameters: b, c, A_B, f_B, and φ. This expression is fitted to the segment of the experimental reflectivity signal, and the zero-crossing point $t_0^{(j)}$, satisfying $\sin(2\pi f_B t_0^{(j)} + \varphi) = 0$, is calculated. At the second iteration step, the signal is fitted once again by the same function $s(t)$, but this time within a segment $[t_0^{(j)}, t_0^{(j+1)}]$ limited by the two adjacent zero points. As a result, the chain approximation for the slow term and piecewise continuous sine approximation for the Brillouin oscillation are obtained. The values of $f_B(t_j)$ and $A_B(t_j)$ obtained at the second iteration give the local frequency and amplitude at the time points $t^{(j)} = (t_0^{(j)} + t_0^{(j+1)})/2$.

Extraction of $v(t)$ and $n(t)$. The measurement of the Brillouin frequency at more than two different probe beam incidence angles θ leads to an overdetermined system of equations where unknown parameters are $v(t)$ and $n(t)$. It can be solved by the least-squares method. Time variations of n and v were parametrized in the form of a power series: $n(t) = n_0 + n_1 t + n_2 t^2/2$ and $v(t) = V_0 + V_1 t + V_2 t^2/2 + V_3 t^3/6$. Seven parameters were determined to provide the best fit for all experimental frequencies $f_B(t_i(\theta))$ simultaneously (Figure 3b). The least-squares problem was regularized using the Tikhonov−Phillips technique.[27] The fitted dependencies of the Brillouin frequency on time are shown in Figure 3b by the solid lines. Each fitting parameter a, evaluated by means of the least-squares technique, has an intrinsic error that is given by $\delta_a^2 = \langle\Sigma\xi_i p_{ai}\rangle^2/(\Sigma p_{ai}^2)^2$, where ξ_i denotes the standard deviation of frequency, $p_{ai} = \partial f_i/\partial a$ characterizes the sensitivity of the frequency to the variations of the parameter a at the time instance t_i, and averaging is performed over all t_i and all incidence angles. Assuming for the estimates that $\langle\xi_i\xi_j\rangle = \sigma^2\delta_{ij}$ with the standard deviation of the frequency noise $\sigma = 0.44$ GHz evaluated from Figure 3b, the standard deviations for all seven fit parameters were calculated, and the results for $n(z)$, $v(z)$, and $U(z)/U(0)$ are depicted in Figure 4b as shaded areas.

Acknowledgment. One of the authors, A.L., was supported by Region Pays de la Loire, France.

Supporting Information Available: Generation of in-depth inhomogeneities in low-k nanoporous film in the process of its UV-assisted thermal curing. Correlation of experimentally revealed nonmonotonic variations of the optical density n along the depth coordinate z of the nanoporous low-k film with nonmonotonic dependence of n on the dose of the UV radiation, which assists film curing. This material is available free of charge *via* the Internet at http://pubs.acs.org.

REFERENCES AND NOTES

1. Garcia, R. Probe Microscopy: Images from below the Surface. *Nat. Nanotechnol.* **2010**, *5*, 101–102.
2. Shekhawat, G. S.; Dravid, V. P. Nanoscale Imaging of Buried Structures via Scanning Near-Field Ultrasound Holography. *Science* **2005**, *310*, 89–92.
3. Werner, M.; Klose, S.; Szuks, F.; Moelle, Ch.; Fecht, H. J.; Johnson, C.; Chalker, P. R.; Buckley-Golder, I. M. High Temperature Young's Modulus of Polycrystalline Diamond. *Diamond Relat. Mater.* **1997**, *6*, 344–347.
4. Lehmann, G.; Schreck, M.; Hou, L.; Lamberts, J.; Hess, P. Dispersion of Surface Acoustic Waves in Polycrystalline Diamond Plates. *Diamond Relat. Mater.* **2001**, *10*, 686–697.
5. van der Drift, A. Evolutionary Selection, A Principle Governing Growth Orientation in Vapour- Deposited Layers. *Philips Res. Rep.* **1967**, *22*, 267–288.
6. Iacopi, F.; Travaly, Y.; Eyckens, B.; Waldfried, C.; Abell, T.; Guyer, E. P.; Gage, D. M. R.; Dauskardt, H.; Sajavaara, T.; Houthoofd, H.; *et al.* Short-Ranged Structural Rearrangement and Enhancement of Mechanical Properties of Organosilicate Glasses Induced by Ultraviolet Radiation. *J. Appl. Phys.* **2006**, *99*, 053511.
7. Iacopi, F.; Beyer, G.; Travaly, Y.; Waldfried, C.; Gage, D. M.; Dauskardt, R. H.; Houthoofd, K.; Jacobs, P.; Adriaensens, P.; Schulze, K.; *et al.* Thermomechanical Properties of Thin Organosilicate Glass Films Treated with Ultraviolet-Assisted Cure. *Acta Mater.* **2007**, *55*, 1407–1414.
8. Kim, T.; Tsuji, N.; Matsushita, K.; Kobayashi, N.; Chumakov, D.; Geisler, H.; Zschech, E.; Dauskardt, R. H. Tuning Depth Profiles of Organosilicate Films with Ultraviolet Curing. *J. Appl. Phys.* **2008**, *104*, 074113.
9. Prager, L.; Marsik, P.; Wennrich, L.; Baklanov, M. R.; Naumov, S.; Pistol, L.; Schneider, D.; Gerlach, J. W.; Verdonck, P.; Buchmeiser, M. R. Effect of Pressure on Efficiency of UV

Curing of CVD-Derived Low-k Material at Different Wavelengths. *Microelectron. Eng.* **2008**, *85*, 2094–2097.
10. Marsik, P.; Verdonck, P.; De Roest, D.; Baklanov, M. R. Porogen Residues Detection in Optical Properties of Low-k Dielectrics Cured by Ultraviolet Radiation. *Thin Solid Films* **2010**, *518*, 4266–4272.
11. Belleville, P.; Bonnin, C.; Priotton, J. −J. Room-Temperature Mirror Preparation Using Sol-Gel Chemistry and Laminar-Flow Coating Technique. *J. Sol-Gel. Sci. Technol.* **2000**, *19*, 223–226.
12. Bhushan, B. *Scanning Probe Microscopy in Nanoscience and Nanotechnology*; Springer: Berlin, 2010.
13. Reimer, L.; Kohl, H. *Transmission Electron Microscopy: Physics of Image Formation*; Springer: Berlin, 2008.
14. Benninghoven, A.; Rüdenauer, F. G.; Werner, V. *Secondary Ion Mass Spectrometry: Basic Concepts, Instrumental Aspects, Applications, and Trends*; Wiley: New York, 1987.
15. Bilewska, K.; Wolna, E.; Edely, M.; Ruello, P.; Szade, J. $EuNiO_3$ Thin Films−Growth and Characterization. *J. Phys.: Conf. Series.* **2011**, *289*, 012014.
16. Rabe, U.; Arnold, W. Acoustic Microscopy by Atomic Force Microscopy. *Appl. Phys. Lett.* **1994**, *64*, 1493–1495.
17. Sahin, O.; Mogonov, S.; Su, S.; Quate, C. F.; Soolgaard, O. An Atomic Force Microscope Tip Designed to Measure Time-Varying Nanomechanical Forces. *Nat. Nanotechnol.* **2007**, *2*, 507–514.
18. Tetard, L.; Passian, A.; Thundat, T. New Modes for Subsurface Atomic Force Microscopy Through Nanomechanical Coupling. *Nat. Nanotechnol.* **2010**, *5*, 105–109.
19. Martinez, N. F.; Patil, S.; Lozano, J. R.; Garcia, R. Enhanced Compositional Sensitivity in Atomic Force Microscopy by the Excitation of the First Two Flexural Modes. *Appl. Phys. Lett.* **2006**, *89*, 153115.
20. Mechri, C.; Ruello, P.; Breteau, J. M.; Baklanov, M. R.; Verdonck, P.; Gusev, V. Depth-Profiling of Elastic Inhomogeneities in Transparent Nanoporous Low-k Materials by Picosecond Ultrasonic Interferometry. *Appl. Phys. Lett.* **2009**, *95*, 091907.
21. Thomsen, C.; Grahn, H. T.; Maris, H. J.; Tauc, J. Surface Generation and Detection of Phonons by Picosecond Light Pulses. *Phys. Rev. B* **1986**, *34*, 4129–4132.
22. Cote, R.; Devos, A.; Côte, R.; Devos, A. Refractive Index, Sound Velocity and Thickness of Thin Transparent Films from Multiple Angles Picosecond Ultrasonics. *Rev. Sci. Instrum.* **2005**, *76*, 053906.
23. Mechri, C.; Ruello, P.; Gusev, V.; Breteau, J.-M.; Mounier, D.; Henderson, M.; Gibaud, A.; Dourdain, S. Evaluation of Elastic Properties of Nanoporous Silicon Oxide Thin Films by Picosecond Laser Ultrasonics. *Eur. Phys. J. Special Top.* **2008**, *153*, 211–213.
24. Brekhovskikh, L. M.; Godin, O. A. *Acoustics of Layered Media I: Plane and Quasi-Plane Waves*; Springer-Verlag: Berlin, 1990.
25. KravtsovYu., A.; Orlov, Yu. I. *Geometrical Optics in Inhomogeneous Media*; Springer-Verlag: Berlin, 1989.
26. Gusev, V. Laser Hypersonics in Fundamental and Applied Research. *Acta Acust. Acust.* **1986**, *82*, S37–S45.
27. Tikhonov, A. N.; Arsenin, V. Y. *Solutions of Ill-Posed Problems*; Wiley: New York, 1977.